materials

MDPI

Article

Formation of TiB_2–$MgAl_2O_4$ Composites by SHS Metallurgy

Chun-Liang Yeh * and Fu-You Zheng

Department of Aerospace and Systems Engineering, Feng Chia University, Taichung 40724, Taiwan
* Correspondence: clyeh@fcu.edu.tw; Tel.: +886-4-2451-7250 (ext. 3963)

Abstract: TiB_2–$MgAl_2O_4$ composites were fabricated by combustion synthesis involving metallothermic reduction reactions. Thermite reagents contained Al and Mg as dual reductants and TiO_2 or B_2O_3 as the oxidant. The reactant mixtures also comprised elemental Ti and boron, as well as a small amount of Al_2O_3 or MgO to serve as the combustion moderator. Four reaction systems were conducted and all of them were exothermic enough to proceed in the mode of self-propagating high-temperature synthesis (SHS). The reaction based on B_2O_3/Al/Mg thermite and diluted with MgO was the most exothermic, while that containing TiO_2/Al/Mg thermite and Al_2O_3 as the diluent was the least. Depending on different thermites and diluents, the combustion front temperatures in a range from 1320 to 1720 °C, and combustion wave velocity from 3.9 to 5.7 mm/s were measured. The XRD spectra confirmed in situ formation of TiB_2 and $MgAl_2O_4$. It is believed that $MgAl_2O_4$ was synthesized through a combination reaction between Al_2O_3 and MgO, both of which can be totally or partially produced from the metallothermic reduction of B_2O_3 or TiO_2. The microstructure of the TiB_2–$MgAl_2O_4$ composite exhibited fine TiB_2 crystals surrounded by large densified $MgAl_2O_4$ grains. This study demonstrated an energy-saving and efficient route for fabricating $MgAl_2O_4$-containing composites.

Keywords: $MgAl_2O_4$; TiB_2; metallothermic reduction; SHS powder metallurgy; combustion wave propagation

check for updates

Citation: Yeh, C.-L.; Zheng, F.-Y. Formation of TiB_2–$MgAl_2O_4$ Composites by SHS Metallurgy. *Materials* **2023**, *16*, 1615. https://doi.org/10.3390/ma16041615

Academic Editor: Dina V. Dudina

Received: 30 January 2023
Revised: 13 February 2023
Accepted: 13 February 2023
Published: 15 February 2023

1. Introduction

TiB_2 has been one of the most studied ultra-high temperature ceramics (UHTCs) due to its unique properties, including a high melting point (3225 °C), high hardness (33 MPa), high Young's modulus (530 MPa), excellent wear and oxidation resistance, thermal shock resistance, chemical inertness, and good electric conductivity [1–3]. Combination of these properties makes TiB_2 an ideal candidate for use in ballistic armors, crucibles, metal evaporation boats, cutting tools, wear resistance parts, and cathodes for alumina smelting [4–6]. Many ceramic phases, such as Al_2O_3, SiC, B_4C, and $MgAl_2O_4$, have been considered as the reinforcement to improve fracture toughness, oxidation resistance, heat resistance, and mechanical strength of the TiB_2-based composites [7–10]. Moreover, a recent study showed that TiB_2–Al_2O_3–$MgAl_2O_4$ composite possesses temperature insensitive and enhanced microwave absorption properties [11]. Magnesium aluminate spinel, $MgAl_2O_4$, as an additive has been rarely studied, possibly because the fabrication of $MgAl_2O_4$ via either the direct solid-state reaction of oxides or wet chemical methods requires multiple steps that are complicated and time-consuming [12–14]. However, $MgAl_2O_4$ is an attractive component due to its high melting point, chemical inertness, high hardness, corrosion resistance, high mechanical strength, and low cost [12].

Among various fabrication routes for preparing multiphasic ceramics, metallothermic reduction reactions (i.e., thermite reactions) combined with combustion synthesis have been recognized as a promising technique for in situ formation of $MgAl_2O_4$-containing composites [15]. Combustion synthesis in the mode of self-propagating high-temperature synthesis (SHS), which is based on strongly exothermic reactions, has merits of low energy consumption, short reaction time, simple equipment and operation, high-purity products, and in situ

formation of composite components [16–18]. Moreover, aluminothermic and magnesiothermic reduction reactions have Al_2O_3 and MgO as their respective by-products, both of which are precursors for the formation of $MgAl_2O_4$. Consequently, Omran et al. [19] applied the reduction-based SHS technique to produce $MgAl_2O_4$–W–W_2B composites through magnesiothermic reduction of B_2O_3 and WO_3 in the presence of Al_2O_3. Zaki et al. [20] synthesized $MoSi_2$– and Mo_5Si_3–$MgAl_2O_4$ composites by SHS with a reducing stage from raw materials consisting of MoO_3, SiO_2, and Al as aluminothermic reagents and MgO as a precursor. Similarly, MgO was added into the reactive mixture of TiO_2, B_2O_3, and Al to fabricate TiB_2–$MgAl_2O_4$ composites by thermitic combustion synthesis [21]. Generally, most of the previous studies on the formation of $MgAl_2O_4$-containing composites had prior addition of one of two precursors (Al_2O_3 or MgO) in the green samples.

This study represents the first attempt to prepare TiB_2–$MgAl_2O_4$ composites from the SHS powder metallurgy simultaneously involving aluminothermic and magnesiothermic reduction of TiO_2 or B_2O_3. Only a small amount of Al_2O_3 or MgO was included in the reactive mixture to serve as the combustion moderator and part of the precursors for the formation of $MgAl_2O_4$. Four SHS reaction systems formulated with different metallothermic reagents and combustion diluents were investigated. In this work, combustion exothermicity and kinetics of the combustion wave of the SHS process, as well as compositions and microstructures of the final products were explored.

2. Materials and Methods

The starting materials adopted by this study included TiO_2 (Acros Organics, Geel, Belgium, 99.5%), B_2O_3 (Acros Organics, 99%), Al_2O_3 (Alfa Aesar, Haverhill, MA, USA, 99%), MgO (Acros Organics, 99.5%), Al (Showa Chemical Co., Tokyo, Japan, <45 µm, 99.9%), Mg (Alfa Aesar, <45 µm, 99.8%), Ti (Alfa Aesar, <45 µm, 99.8%), and amorphous boron (Noah Technologies, San Antonio, TX, USA, <1 µm, 93.5%). Four SHS reactions were formulated for the synthesis of $3TiB_2$–$MgAl_2O_4$ composites. Two metallothermic reagents (i.e., thermites) were considered; one is composed of TiO_2, Al, and Mg, as shown in Equations (1) and (2), and the other comprises B_2O_3, Al, and Mg, as in Equations (3) and (4). Due to strong exothermicity of combustion, Al_2O_3 with an amount of 0.3 mol. was included in Equations (1) and (3) as the combustion moderator (or combustion diluent) in order to attain stable propagation of the combustion wave. The pre-added Al_2O_3 also acted as part of the precursor for the synthesis of $MgAl_2O_3$. Likewise, an equal amount of MgO was adopted by Equations (2) and (4) and MgO played the same role as Al_2O_3 in Equations (1) and (3).

$$(1.55TiO_2 + 1.4Al + Mg) + 0.3Al_2O_3 + 1.45Ti + 6B \rightarrow 3TiB_2 + MgAl_2O_4 \quad (1)$$

$$(1.85TiO_2 + 2Al + 0.7Mg) + 0.3MgO + 1.15Ti + 6B \rightarrow 3TiB_2 + MgAl_2O_4 \quad (2)$$

$$(1.033B_2O_3 + 1.4Al + Mg) + 0.3Al_2O_3 + 3Ti + 3.934B \rightarrow 3TiB_2 + MgAl_2O_4 \quad (3)$$

$$(1.233B_2O_3 + 2Al + 0.7Mg) + 0.3MgO + 3Ti + 3.534B \rightarrow 3TiB_2 + MgAl_2O_4 \quad (4)$$

Combustion exothermicity of the above four reactions, Equations (1)–(4), was evaluated by calculating their adiabatic combustion temperatures (T_{ad}) from the following energy balance equation [17,22] with thermochemical data taken from [23].

$$\Delta H_r + \int_{298}^{T_{ad}} \sum n_j c_p(P_j) dT + \sum_{298-T_{ad}} n_j L(P_j) = 0$$

where ΔH_r is the reaction enthalpy at 298 K, c_p and L are the heat capacity and latent heat, n_j is the stoichiometric coefficient, and P_j refers to the product component.

The SHS experiments were conducted in a windowed combustion chamber filled with Ar at 0.25 MPa. Reactant powders were well mixed in a tubular ball mill and then uniaxially compressed into cylindrical test specimens with a diameter of 7 mm, a height of

12 mm, and a relative density of 55%. The sample compact was ignited by an electrically heated tungsten coil. An R-type bare-wire thermocouple (Pt/Pt-13%Rh) with a bead size of 125 μm was used to measure the combustion temperature. The propagation velocity of combustion wave (V_f) was determined by the time derivative of the flame-front trajectory constructed from the recorded series of combustion images. Phase compositions of the products were identified by an X-ray diffractometer (XRD, Bruker D2 Phaser, Karlsruhe, Germany). Microstructures and constituent elements of the products were examined by the scanning electron microscopy (SEM, Hitachi, Tokyo, Japan, S3000H) and energy dispersive spectroscopy (EDS). Details of the experimental methods were reported elsewhere [24].

3. Results and Discussion

3.1. Combustion Exothermicity of Reduction-Based SHS Reactions

Figure 1 presents the calculated ΔH_r and T_{ad} of reactions Equations (1)–(4) and shows that Equation (4) has the highest values while Equation (1) has the lowest ones. Both ΔH_r and T_{ad} increase from Equations (1)–(4). Specifically, the values of T_{ad} are 2530 K, 2595 K, 2783 K, 2897 K for Equation (1)–(4), respectively. A comparison between Equations (1) and (2) revealed that the combustion moderator Al_2O_3 appeared to impose a stronger dilution effect on combustion than MgO, which led to a lower T_{ad} for Equation (1) than Equation (2). Similar results were observed in Equations (3) and (4). These findings could also be explained by the fact that metallothemic reduction of TiO_2 or B_2O_3 by Al is more exothermic than that by Mg [15,25].

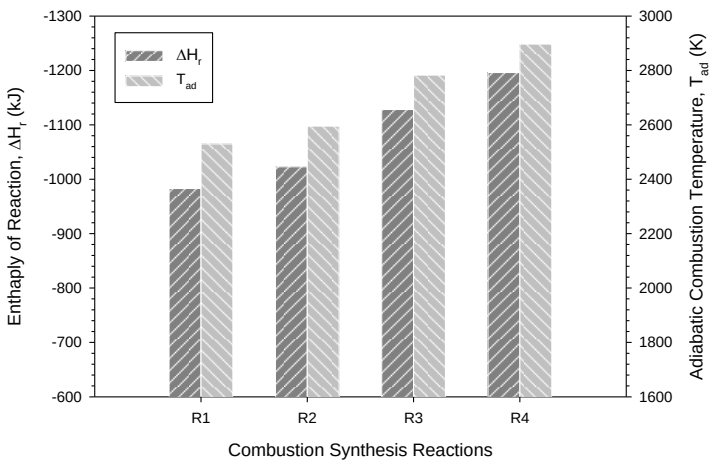

Figure 1. Enthalpies of reaction (ΔH_r) and adiabatic combustion temperatures (T_{ad}) of Equation (1)–(4) for the synthesis of $3TiB_2$–$MgAl_2O_4$ composites.

On the other hand, because the B_2O_3-based thermite is more energetic than the one using TiO_2 [25], Equation (3) has a higher T_{ad} than Equation (1). Similarly, Equation (4) has a higher T_{ad} than Equation (2). According to the calculated T_{ad}, it is realized that the thermite oxidants (i.e., B_2O_3 versus TiO_2) have a more pronounced influence on combustion exothermicity than the diluent oxides (i.e., Al_2O_3 versus MgO).

3.2. Combustion Temperature and Self-Propagating Velocity

Two series of the SHS processes recorded from reactions Equations (1) and (3) are illustrated in Figure 2a,b, respectively. It is apparent that upon ignition, the reaction was initiated and characterized by a self-sustaining combustion wave. More intense combustion accompanied with a faster combustion wave was observed in Figure 2b, when compared with that in Figure 2a. Combustion luminosity and flame spreading speed reflected the degree of reaction exothermicity. As mentioned above, B_2O_3/Al/Mg-based Equation (3) is more energetic than TiO_2/Al/Mg-based Equation (1). Similar combustion behavior was also noticed in Equations (2) and (4).

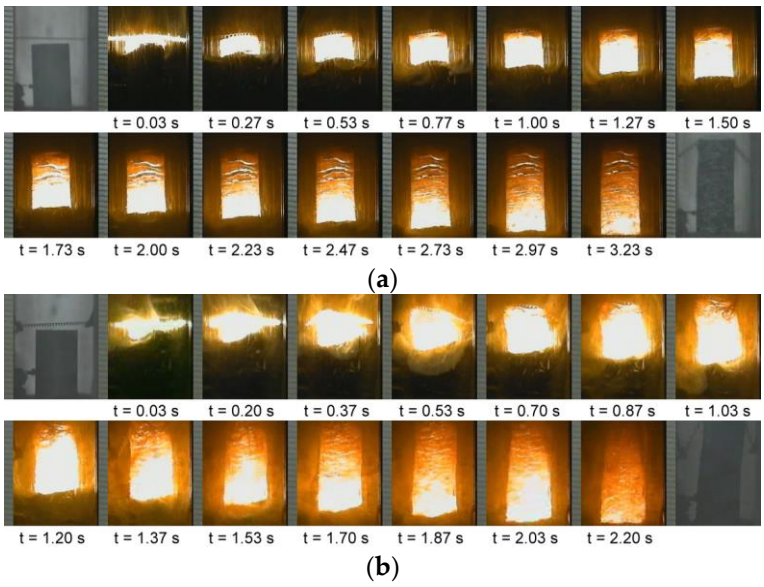

Figure 2. Time sequences of recorded SHS images illustrating self-sustaining combustion wave of (**a**) Equation (1) and (**b**) Equation (3).

Figure 3 depicts typical combustion temperature profiles measured from four different reactions. All profiles exhibit a steep temperature rise followed by a rapid descent, which is characteristic of the SHS reaction that features a fast combustion wave and a thin reaction zone. The peak value is considered as the combustion front temperature (T_c). When compared with pinnacles in the contours of Equations (1) and (2), sharper peaks were detected in the profiles of Equations (3) and (4). This implied a faster combustion wave in Equations (3) and (4). As shown in Figure 3, the values of T_c from Equation (1)–(4) in ascending order are 1348 °C, 1445 °C, 1660 °C, and 1736 °C. It should be noted that the measured combustion front temperatures are in agreement with the calculated reaction exothermicity.

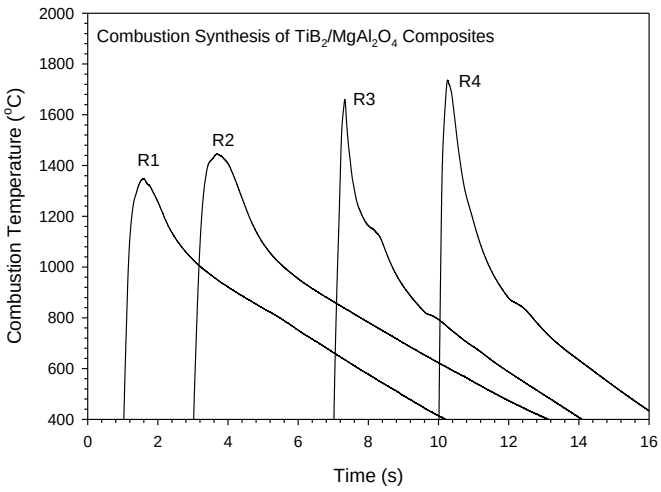

Figure 3. Typical combustion temperature profiles measured from Equation (1)–(4) for the synthesis of $3TiB_2$–$MgAl_2O_4$ composites.

It is useful to note in Figure 3 that the curves of Equations (3) and (4) have a shape peak with a pronounced shoulder. The shape peak was a result of the fast combustion wave. The pronounced shoulder could be caused by the occurrence of volumetric synthesis reactions after the passage of the rapid combustion wave.

Figure 4 plots the measured combustion wave propagation velocities (V_f) and temperatures (T_c) of four reactions. The rising trend of V_f from Equations (1)–(4) is consistent with that of T_c. This can be understood by the fact that the propagation of combustion wave is essentially governed by layer-by-layer heat transfer from the reaction zone to unreacted region, and therefore, is subject to the combustion front temperature. As presented in Figure 4, the average combustion velocities are 3.9, 4.7, 5.1, and 5.7 mm/s for Equations (1)–(4), respectively. It is worth noting that the measured combustion temperature not only justified the reaction exothermic analysis, but confirmed the temperature dependence of combustion wave velocity.

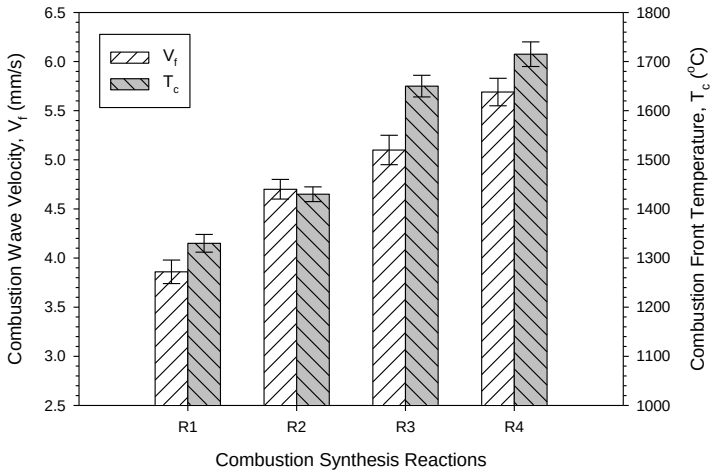

Figure 4. Combustion wave velocity (V_f) and combustion front temperature (T_c) measured from Equation (1)–(4) for the synthesis of $3TiB_2$–$MgAl_2O_4$ composites.

3.3. Composition and Microstructure Analyses of Synthesized Products

The XRD spectra of the final products synthesized from Equations (1) and (2) are shown in Figure 5a,b, respectively. Both indicated the formation of TiB_2 and $MgAl_2O_4$ along with two minor phases, magnesium titanate ($MgTiO_3$) and MgO. It is believed that $MgAl_2O_4$ was synthesized through a combination reaction between Al_2O_3 and MgO. Equation (1) and (2) were formulated with the same thermite reagents of TiO_2, Al, and Mg, but diluted by different metal oxides. That is, Al_2O_3 was partly pre-added and partly thermite-produced, while MgO was completely generated from the reduction of TiO_2 by Mg in Equation (1). In contrast, the required Al_2O_3 in Equation (2) was entirely produced from the reduction of TiO_2 by Al, but MgO was supplied in part from prior addition and in part from the reduction of TiO_2 by Mg. For both Equations (1) and (2), TiB_2 was synthesized from the reaction of elemental boron with reduced and metallic Ti.

Traces of MgO suggested an incomplete reaction due probably to the relatively low reaction temperatures of Equations (1) and (2). The presence of $MgTiO_3$ in the final products of Equations (1) and (2) could be attributed to the reaction of MgO with the thermite oxidant TiO_2 [26,27]. The formation of $MgTiO_3$ in the SHS-produced TiB_2–$MgAl_2O_4$ composites was also observed by Radishevskaya et al. [10] using Ti, boron, and $MgAl_2O_4$ as their starting materials and a partial decomposition of $MgAl_2O_4$ during combustion synthesis was considered as a possible route resulting in the formation of $MgTiO_3$.

The presence of MgO along with no detection of Al_2O_3 in the final products of Equations (1) and (2) suggested that the as-synthesized $MgAl_2O_4$ is an Al_2O_3-rich spinel. The formation of $MgTiO_3$ could also result in the production of Al_2O_3-rich spinel. According to Naghizadeh et al. [28], magnesium titanate compounds ($MgTiO_3$ and Mg_2TiO_4) were identified in the phase evolution of $MgAl_2O_4$ produced from TiO_2-containing samples and stoichiometric $MgAl_2O_4$ spinel shifted toward the Al_2O_3-rich type. Due to the formation of $MgTiO_3$, the amount of TiB_2 formed in the composite should be less than the stoichiometric amount.

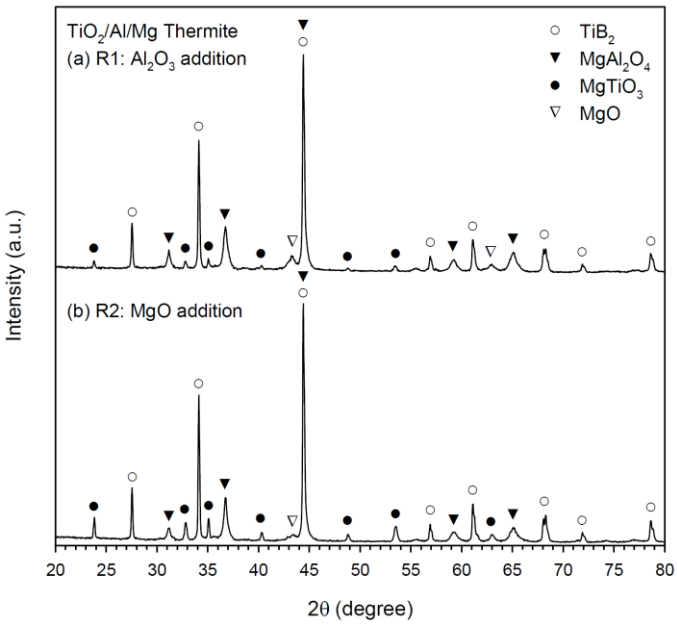

Figure 5. XRD patterns of $TiB_2/MgAl_2O_4$ composites obtained from SHS reactions of (**a**) Equation (1) and (**b**) Equation (2).

Figure 6a,b exhibits the XRD patterns of the synthesized composites from Equations (3) and (4), respectively. In addition to TiB_2 and $MgAl_2O_4$, a small amount of $MgTiO_3$ was identified. The formation of $MgAl_2O_4$ from a combination reaction between Al_2O_3 and MgO was proved. Both Al_2O_3 and MgO can be totally or partially produced from the reduction of B_2O_3 by Al and Mg. For Equations (3) and (4) containing B_2O_3/Al/Mg-based thermite, TiB_2 was produced from the reaction of metallic Ti with reduced and elemental boron. Moreover, the formation of $MgTiO_3$ in Equations (3) and (4) might involve some interaction of Ti with B_2O_3 to form TiO_2 which further reacted with MgO. Unlike that in Equations (1) and (2), MgO was no longer detected in the final products of Equations (3) and (4).

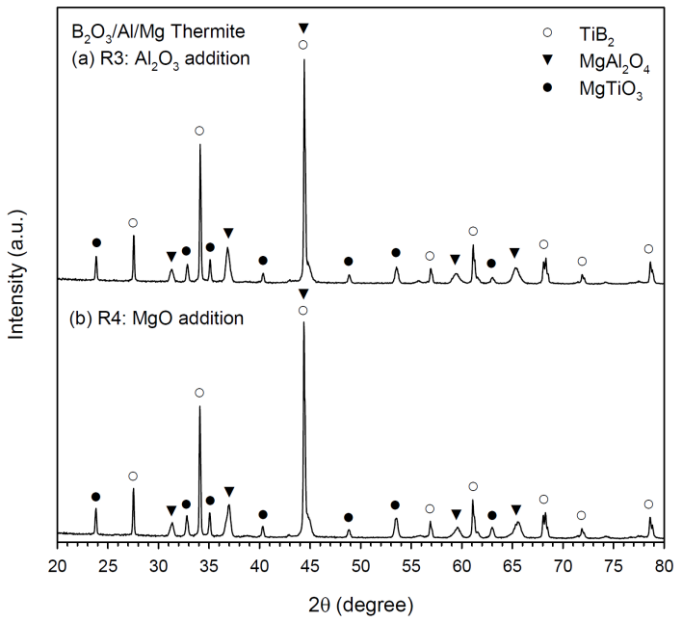

Figure 6. XRD patterns of $TiB_2/MgAl_2O_4$ composites obtained from SHS reactions of (**a**) Equation (3) and (**b**) Equation (4).

$MgTiO_3$ ceramic has been proved to be an excellent dielectric material, owing to its high dielectric constant, low dielectric loss, high value of quality factors, and good temperature stability [29,30]. It is believed that a trace amount of $MgTiO_3$ as a minor phase existed in the as-synthesized TiB_2-$MgAl_2O_4$ products has no effect on the refractory properties of the composites. However, removal of $MgTiO_3$ from the TiB_2-$MgAl_2O_4$ composite would be difficult, since it could combine with $MgAl_2O_4$ in a solid solution form [28].

The SEM image shown in Figure 7 illustrates the microstructure of fracture surface of the product synthesized from Equation (1) which contains a TiO_2/Al/Mg-based thermite. The morphology displays several large and solidified $MgAl_2O_4$ aggregates of 5–15 μm surrounded by fine-grain TiB_2 crystals with a particle size of about 1–2 μm. Moreover, EDS analysis of two characteristic regions in the product surface indicates that the atomic ratios of Ti:B = 35.2:64.8 and Mg:Al:O = 13.1:28.1:58.8 match well with the stoichiometries of TiB_2 and $MgAl_2O_4$, respectively.

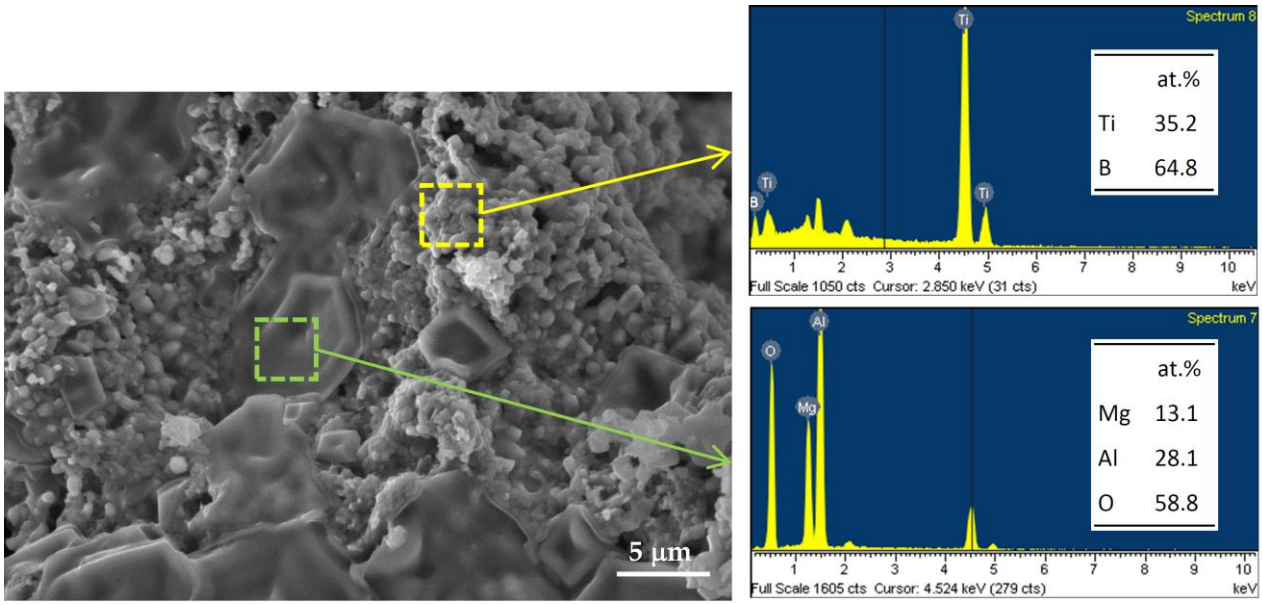

Figure 7. SEM image and EDS spectra of TiB_2/$MgAl_2O_4$ composite obtained from the SHS reaction of Equation (1).

For the final product of B_2O_3/Al/Mg-based Equation (4), the microstructure and elemental ratios of the components are presented in Figure 8. As can be seen, $MgAl_2O_4$ was formed as large densified aggregates of around 20 μm and TiB_2 crystals were in a short-rod form with a length of 2–4 μm or in a shape of fine grains of 1–2 μm. Based on the EDS analysis, the atomic ratio of the selected area in an aggregate is Mg:Al:O = 15.1:30.6:54.3 that is reasonably close to $MgAl_2O_4$. Short-rod crystals have a composition of Ti:B = 34.3:65.7, which certainly is TiB_2.

In summary, the addition of $MgAl_2O_4$ into TiB_2 enhanced the refractory properties, such as the high-temperature oxidation and corrosion resistance and thermal shock resistance [10,31,32]. Like many sintering aids, $MgAl_2O_4$ as an additive could improve densification of TiB_2 ceramics and reduce sintering temperatures [33,34]. The abnormal grain growth could be efficiently prevented during the sintering process. As a result, it is more likely to obtain a uniform grain distribution.

Moreover, the TiB_2-$MgAl_2O_4$ composite is a promising high-temperature microwave absorption material with a reflection loss less than –5 dB at 8.2–18.0 GHz in the temperature range of 25 °C to 1100 °C [11]. The composite also exhibits an extremely high tolerance against intense irradiation in harsh environments [35,36]. Therefore, the potential uses of the TiB_2-$MgAl_2O_4$ composite might include heat-resistant coatings, nozzles and nose cones

of supersonic jets, microwave absorption components, diagnostic or detector windows in fusion devices, target materials in the nuclear applications, etc., [11,35,36].

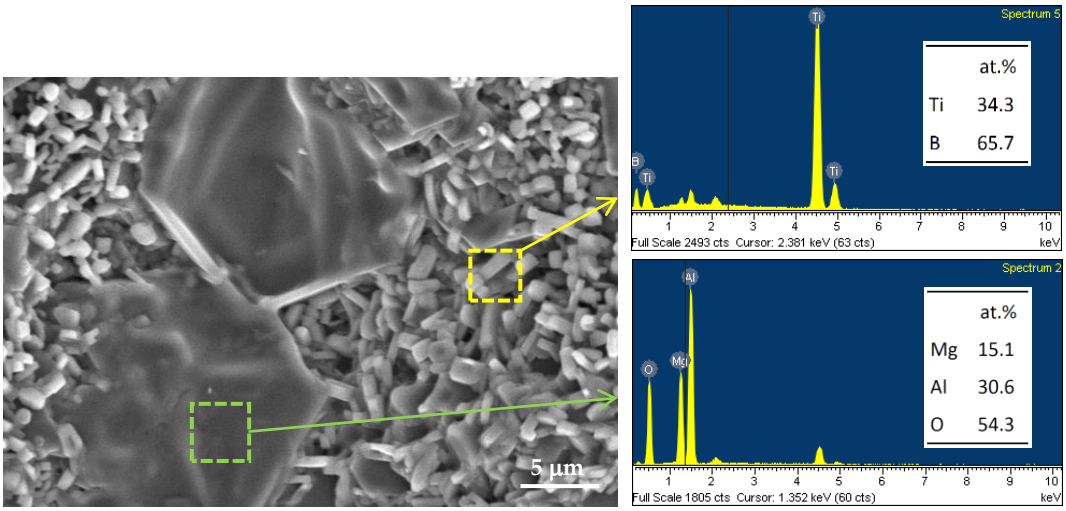

Figure 8. SEM image and EDS spectra of $TiB_2/MgAl_2O_4$ composite obtained from the SHS reaction of Equation (4).

4. Conclusions

In situ formation of $3TiB_2$–$MgAl_2O_4$ composites was conducted by combustion synthesis combined with metallothermic reduction reactions involving Al and Mg as dual reductants. Thermite reagents with different oxidants were considered; one utilized TiO_2 and the other B_2O_3. The reactant mixtures also contained elemental Ti and boron. This study in total completed four SHS reactions, within which a small amount of Al_2O_3 or MgO was included in the reactive mixture to serve as the combustion moderator and part of the precursors for the formation of $MgAl_2O_4$. The overall synthesis reaction was exothermic enough to proceed in the SHS mode. An energy-saving and efficient fabrication route for the formation $MgAl_2O_4$-containing composites was demonstrated.

The analysis of combustion exothermicity indicated that the SHS reaction containing B_2O_3/Al/Mg-based thermites was more energetic than that adopting TiO_2 as the oxidant. Prior addition of Al_2O_3 had a greater cooling effect on combustion than that of MgO. Depending on different thermites and diluents, the measured combustion front temperatures ranged from 1320 to 1720 °C, and combustion wave velocity from 3.9 to 5.7 mm/s. The temperature dependence of combustion wave velocity was justified. The XRD analysis confirmed in situ formation of TiB_2 and $MgAl_2O_4$. A small amount of $MgTiO_3$ was found as the impurity. It is believed that $MgAl_2O_4$ was synthesized through a combination reaction between Al_2O_3 and MgO, both of which can be totally or partially produced from the metallothermic reduction of B_2O_3 or TiO_2. The microstructure of the synthesized composite exhibited that $MgAl_2O_4$ was surrounded by closely packed TiB_2 grains. $MgAl_2O_4$ was formed as densified aggregates with a size of 5–20 µm. TiB_2 crystals were produced in a shape of short rods of 2–4 µm and fine grains of 1–2 µm.

Author Contributions: Conceptualization, C.-L.Y.; methodology, C.-L.Y. and F.-Y.Z.; validation, C.-L.Y. and F.-Y.Z.; formal analysis, C.-L.Y. and F.-Y.Z.; investigation, C.-L.Y. and F.-Y.Z.; resources, C.-L.Y.; data curation, C.-L.Y. and F.-Y.Z.; writing—original draft preparation, C.-L.Y. and F.-Y.Z.; writing—review and editing, C.-L.Y.; supervision, C.-L.Y.; project administration, C.-L.Y.; funding acquisition, C.-L.Y. All authors have read and agreed to the published version of the manuscript.

Funding: This research work was funded by the National Science and Technology Council of Taiwan under the grant of NSTC 110-2221-E-035-042-MY2.

Institutional Review Board Statement: Not applicable.

Informed Consent Statement: Not applicable.

Data Availability Statement: Data presented in this study are available in the article.

Conflicts of Interest: The authors declare no conflict of interest.

References

1. Wilkins, J.M.L. *Boron and Refractory Borides*; Matkovich, V.I., Ed.; Springer: New York, NY, USA, 1977; p. 633.
2. Balcı, Ö.; Burkhardt, U.; Schmidt, M.; Hennicke, J.; Yağcı, M.B.; Somer, M. Densification, microstructure and properties of TiB_2 ceramics fabricated by spark plasma sintering. *Mater. Charact.* **2018**, *145*, 435–443. [CrossRef]
3. Ramesh, B.; Showman, E.; Abraar, S.A.M.; Saxena, K.K.; Tharwan, M.Y.; Alsaadi, N.; Al Sofyani, S.; Elsheikh, A.H. Microstructure, mechanical characteristics, and wear performance of spark plasma sintered TiB_2–Si_3N_4 as affected by B_4N doping. *Materials* **2022**, *15*, 7096. [CrossRef] [PubMed]
4. Munro, R.G. Material properties of titanium diboride. *J. Res. Natl. Inst. Stand. Technol.* **2000**, *105*, 709–720. [CrossRef] [PubMed]
5. Vaferi, K.; Nekahi, S.; Vajdi, M.; Moghanlou, F.S.; Shokouhimehr, M.; Motallebzadeh, A.; Sha, J.; Asl, M.S. Heat transfer, thermal stress and failure analyses in a TiB_2 gas turbine stator blade. *Ceram. Int.* **2019**, *45*, 19331–19339. [CrossRef]
6. Sulima, I.; Hyjek, P.; Podsiadło, M.; Boczkal, S. Effect of zirconium diboride and titanium diboride on the structure and properties of 316L steel-based composites. *Materials* **2023**, *16*, 439. [CrossRef]
7. Popov, A.Y.; Sivak, A.A.; Borodianska, H.Y.; Shabalin, I.L. High toughness TiB_2–Al_2O_3 composite ceramics produced by reactive hot pressing with fusible components. *Adv. Appl. Ceram.* **2015**, *114*, 178–182. [CrossRef]
8. Kozień, D.; Czekaj, I.; Gancarz, P.; Ziąbka, M.; Wieczorek, W.; Pasiut, K.; Zientara, D.; Pędzich, Z. Ceramic matrix composites obtained by the reactive sintering of boron carbide with intermetallic compounds from the Ti-Si system. *Materials* **2022**, *15*, 8657. [CrossRef]
9. Li, Z.; Chen, Q.; Jiao, B.; Wang, Q.; Zhang, H.; Jia, Q.; Zhang, S.; Liu, J. Direct laser powder-bed fusion additive manufacturing of complex-shaped TiB_2-B_4C composite with ultra-fine eutectic microstructure and outstanding mechanical performances. *J. Eur. Ceram. Soc.* **2023**, *43*, 1230–1236. [CrossRef]
10. Radishevskaya, N.; Lepakova, O.; Karakchieva, N.; Nazarova, A.; Afanasiev, N.; Godymchuk, A.; Gusev, A. Self-propagating high temperature synthesis of TiB_2–$MgAl_2O_4$ composites. *Metals* **2017**, *7*, 295. [CrossRef]
11. Yang, J.; Liu, X.; Gong, W.; Wang, T.; Wang, X.; Gong, R. Temperature-insensitive and enhanced microwave absorption of $TiB_2/Al_2O_3/MgAl_2O_4$ composites: Design, fabrication, and characterization. *J. Alloys Compd.* **2022**, *894*, 162144. [CrossRef]
12. Ganesh, I. A review on magnesium aluminate ($MgAl_2O_4$) spinel: Synthesis, processing and applications. *Int. Mater. Rev.* **2013**, *58*, 63–112. [CrossRef]
13. Corlett, C.A.; Frontzek, M.D.; Obradovic, N.; Watts, J.L.; Fahrenholtz, W.G. Mechanical activation and cation site disorder in $MgAl_2O_4$. *Materials* **2022**, *15*, 6422. [CrossRef]
14. Yuan, L.; Tian, C.; Yan, X.; He, X.; Liu, Z.; Wen, T.; Jin, E.; Yu, J. Preparation of porous $MgAl_2O_4$ ceramics by a novel pectin gel-casting process. *J. Aust. Ceram. Soc.* **2021**, *57*, 1049–1055. [CrossRef]
15. Yeh, C.L.; Chen, M.C.; Shieh, T.H. Formation of silicide/spinel ceramic composites via Al- and Mg-based thermitic combustion synthesis. *J. Aust. Ceram. Soc.* **2022**, *58*, 1275–1282. [CrossRef]
16. Levashov, E.A.; Mukasyan, A.S.; Rogachev, A.S.; Shtansky, D.V. Self-propagating high-temperature synthesis of advanced materials and coatings. *Int. Mater. Rev.* **2017**, *62*, 203–239. [CrossRef]
17. Xu, J.; Ma, P.; Zou, B.; Yang, X. Reaction behavior and formation mechanism of ZrB_2 and ZrC from the Ni-Zr-B_4C system during self-propagating high-temperature synthesis. *Materials* **2023**, *16*, 354. [CrossRef]
18. Zakaryan, M.K.; Zurnachyan, A.R.; Amirkhanyan, N.H.; Kirakosyan, H.V.; Antonov, M.; Rodriguez, M.A.; Aydinyan, S.V. Novel pathway for the combustion synthesis and consolidation of boron carbide. *Materials* **2022**, *15*, 5042. [CrossRef]
19. Omran, J.G.; Afarani, M.S.; Sharifitabar, M. Fast synthesis of $MgAl_2O_4$–W and $MgAl_2O_4$–W–W_2B composite powders by self-propagating high-temperature synthesis reactions. *Ceram. Int.* **2018**, *44*, 6508–6513. [CrossRef]
20. Zaki, Z.I.; Mostafa, N.Y.; Rashad, M.M. High pressure synthesis of magnesium aluminate composites with $MoSi_2$ and Mo_5Si_3 in a self-sustaining manner. *Ceram. Int.* **2012**, *38*, 5231–5237. [CrossRef]
21. Zaki, Z.I.; Ahmed, Y.M.Z.; Abdel-Gawad, S.R. In-situ synthesis of porous magnesia spinel/TiB_2 composite by combustion technique. *J. Ceram. Soc. Jpn.* **2009**, *117*, 719–723. [CrossRef]
22. Liang, Y.H.; Wang, H.Y.; Yang, Y.F.; Zhao, R.Y.; Jiang, Q.C. Effect of Cu content on the reaction behaviors of self-propagating high-temperature synthesis in Cu-Ti-B_4C system. *J. Alloys Compd.* **2008**, *462*, 113–118. [CrossRef]
23. Binnewies, M.; Milke, E. *Thermochemical Data of Elements and Compounds*; Wiley-VCH Verlag GmbH: Weinheim, Germany, 2002.
24. Yeh, C.L.; Lin, J.Z. Combustion synthesis of Cr-Al and Cr-Si intermetallics with Al_2O_3 additions from Cr_2O_3-Al and Cr_2O_3-Al-Si reaction systems. *Intermetallics* **2013**, *33*, 126–133. [CrossRef]
25. Wang, L.L.; Munir, Z.A.; Maximov, Y.M. Thermite reactions: Their utilization in the synthesis and processing of materials. *J. Mater. Sci.* **1993**, *28*, 3693–3708. [CrossRef]
26. Singh, J.; Bahel, S. Synthesis of single phase $MgTiO_3$ and influence of Sn^{4+} substitution on its structural, dielectric and electrical properties. *J. Alloys Compd.* **2020**, *816*, 152679. [CrossRef]

27. Cheng, L.; Liu, P.; Qu, S.X.; Cheng, L.; Zhang, H. Microwave dielectric properties of Mg_2TiO_4 ceramics synthesized via high energy ball milling method. *J. Alloys Compd.* **2015**, *623*, 238–242. [CrossRef]
28. Naghizadeh, R.; Rezaie, H.R.; Golestani-Fard, F. Effect of TiO_2 on phase evolution and microstructure of $MgAl_2O_4$ spinel in different atmospheres. *Ceram. Int.* **2011**, *37*, 349–354. [CrossRef]
29. Jo, H.J.; Kim, J.S.; Kim, E.S. Microwave dielectric properties of $MgTiO_3$-based ceramics. *Ceram. Int.* **2015**, *41*, S530–S536. [CrossRef]
30. Thatikonda, S.K.; Goswami, D.; Dobbidi, P. Effects of CeO_2 nanoparticles and annealing temperature on the microwave dielectric properties of $MgTiO_3$ ceramics. *Ceram. Int.* **2014**, *40*, 1125–1131. [CrossRef]
31. Li, Y.; Nan, L.; Ruan, G.; Li, X. Reaction path in the aluminothermic reduction nitridation reaction to synthesize $MgAl_2O_4$/TiN composite. *Ceram. Int.* **2005**, *31*, 825–829. [CrossRef]
32. Liu, X.; Li, K.; Bao, K.; Chen, J.; Zhang, H.; Zhang, S. In-situ synthesis of magnesium aluminate spinel–Zirconium diboride composite powder in magnesium chloride melt. *Ceram. Int.* **2022**, *48*, 11869–11871. [CrossRef]
33. Ma, L.; Yu, J.; Guo, X.; Xie, B.; Gong, H.; Zhang, Y.; Zhaie, Y.; Wu, X. Preparation and sintering of ultrafine TiB_2 powders. *Ceram. Int.* **2018**, *44*, 4491–4495. [CrossRef]
34. Sarkar, R. Additives for magnesium aluminate spinel: A review. *Interceram Refract. Manual* **2011**, *1*, 28–32.
35. Lushchik, A.; Feldbach, E.; Kotomin, E.A.; Kudryavtseva, I.; Kuzovkov, V.N.; Popov, A.I.; Seeman, V.; Shablonin, E. Distinctive features of diffusion-controlled radiation defect recombination in stoichiometric magnesium aluminate spinel single crystals and transparent polycrystalline ceramics. *Sci. Rep.* **2020**, *10*, 7810. [CrossRef] [PubMed]
36. Ananchenko, D.V.; Nikiforov, S.V.; Kuzovkov, V.N.; Popov, A.I.; Ramazanova, G.R.; Batalov, R.I.; Bayazitovc, R.M.; Novikov, H.A. Radiation-induced defects in sapphire single crystals irradiated by a pulsed ion beam. *Nucl. Instrum. Methods Phys. Res. B* **2020**, *466*, 1–7. [CrossRef]